Quantitative low-energy electron diffraction analysis of MnO(100) films grown on Ag(100)

E. A. Soares,* R. Paniago, V. E. de Carvalho, E. L. Lopes, G. J. P. Abreu, and H.-D. Pfannes
Departmento de Física, ICEx, Universidade Federal de Minas Gerais, CP702, Belo Horizonte, MG, Brazil
(Received 20 October 2005; revised manuscript received 2 December 2005; published 13 January 2006)

In this work we report on a low-energy electron diffraction (LEED) study of MnO(100) thick films grown on Ag(100) in order to determine their surface geometry. The LEED results indicate a topmost layer rumple of $(4.8\pm2.0)\%$ with the oxygen ions moving towards the vacuum side. These results are in line with other surface structure determinations carried out on the (100) surface of different oxides having rock-salt structure but are in disagreement with MEIS results reported in the literature for the MnO(100) using a MnO single crystal.

DOI: 10.1103/PhysRevB.73.035419 PACS number(s): 61.14.-x, 68.35.-p, 68.47.Gh

I. INTRODUCTION

Oxide surfaces are of great technological interest, e.g., in protective coating, catalysis, single tunnel barriers and others.[1] However, there are much fewer investigations of their surface properties as compared to metals and semiconductors. The investigation of insulator crystals by means of low energy electron diffraction (LEED) is hindered due to surface charging, unless very low electron beam currents are employed. A practical method to avoid this problem is to prepare an insulator ultrathin film on suitable metal substrates. Another problem that arises when using oxide single crystals is the often poor structural quality of the cleaved surfaces. This is specially true for the case of MnO where the cleavage of a single crystal along the (100) plane normally leads to a surface, which consists of pyramids with (111) octahedral faces.[1]

MnO is a 3*d* antiferromagnet transition metal oxide with a Néel temperature of 120 K (Ref. 2) and has rock-salt bulk structure with a lattice constant of 4.445 Å. As reported in the literature,[1] MnO(100) surfaces cleaved in ultra-high-vacuum (UHV) conditions only exhibit a diffuse (1×1) LEED pattern. Polishing the (100) surface followed by annealing at 480 K results in a clear (1×1) diffraction pattern. Subsequent annealing at temperatures between 800 and 1000 K gives rise to (2×2) and (6×6) reconstructions, respectively, but no change of the surface stoichiometry has been measured. A high resolution electron energy loss spectroscopy study performed on MnO(100) single crystals demonstrated that the (100) surface can be selectively oxidized or reduced by annealing under appropriate oxygen partial pressure or in UHV conditions, respectively.[3] Recently, high-resolution medium energy ion scattering (MEIS) was used in order to investigate the surface structure and lattice dynamics of clean MnO(100)(1×1) surfaces prepared by cleavage in N_2 atmosphere followed by annealing in an O_2 partial pressure.[4] The MEIS results favor a rumpled surface with the top-layer Mn atoms moving toward the vacuum side relative to top-layer oxygen atoms. Those results are in agreement with recent *ab initio* calculations[5] but are in disagreement with all other structural studies carried out on (100) surfaces of other oxides having rock-salt structure, except MEIS results for NiO(100).[6] A very detailed study of epitaxial growth of MnO films on Ag(100) was performed by Müller *et al.*[7] It was demonstrated by that study that it is possible to prepare MnO(100) films on a Ag(100) surface with a structural order comparable to the corresponding substrate crystal if the Mn evaporation rate and the oxygen pressure are properly tuned.

In this paper we present a quantitative LEED study of ultrathin (24 and 48 monolayers) manganese mono-oxide films grown on Ag(100). Growth is observed to be nonpseudomorphous and, even at very low coverage, the lattice parameter of the film is the one observed for bulk MnO. In the Sec. II we describe the experimental and theoretical details. The results and discussion are presented in Sec. III and some conclusions are drawn in Sec. IV.

II. EXPERIMENTAL AND THEORETICAL DETAILS

The experiments have been carried out in a VG Escalab UHV system with a base pressure of 1×10^{-10} mbar. The UHV system was equipped with the standard facilities for sample preparation (cleaning, heating and deposition) and sample characterization (Auger, XPS, and UPS) as well as with a computer controlled 4 grid LEED and a RHEED optics. The Ag(100) single crystal was supplied by the Monocrystal Company, with 99.995% purity, presenting a mirror like (100) surface oriented within ±0.5°. The (100) silver surface was cleaned with several cycles of sputtering (Ar^+ ions at 1.0 keV for 30 minutes) and annealing (up to 450 °C for 5 minutes) until no trace of carbon, oxygen, and sulphur contaminations could be detected by XPS and a sharp (1×1) LEED pattern could be observed. MnO(100) layers of thickness of 1, 2, 8, 24, and 48 monolayers (ML) were prepared by evaporating metallic Mn (99.99% purity) in an O_2 partial pressure of 2×10^{-8} mbar at an evaporation rate of 1.0 ML/min following the procedure described by Müller *et al.*[7] During the evaporation the Ag(100) surface was held at room temperature. Since only diffuse (1×1)LEED patterns were observed after the film growths, the MnO(100) films were annealed at 773 K (±50 K) during 5 minutes. After that a well defined LEED pattern was observed for all MnO(100) films. The MnO stoichiometry was checked by the splitting in the 3*s* XPS peak, before and after annealing. The Mn 3*s* splitting has its origin in the interaction of the spin of the remaining electrons in the Mn 3*s* level after the photoemis-

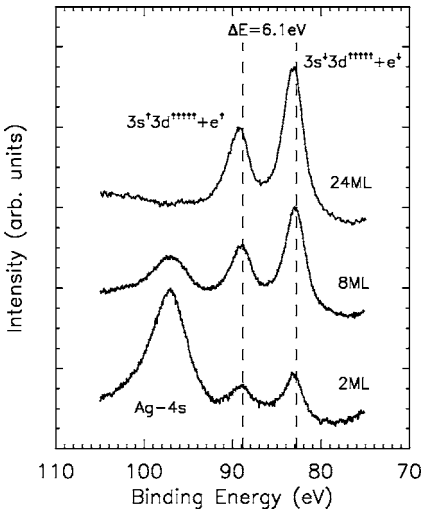

FIG. 1. XPS spectra of the Mn 3*s* splitting of MnO(100) grown on Ag(100). The thicknesses of MnO films are indicated and spectra were collected after annealing at 773 K.

sion process and the resulting Mn 3*d* spin.[7] After each growth, the Ag(100) sample was cleaned by cycles of sputtering and annealing until no trace of Mn and O were detectable by XPS and a new film was grown.

The LEED patterns were collected as a function of the incidence beam energy for the two thickest MnO films using a high-sensitivity CCD camera and an automated data acquisition system. The diffracted intensity as a function of electron energy (LEED-IV curves) for 23 beams was then collected at nominal normal incidence in the range of 50–550 eV. The experimental LEED-IV curves were then normalized by the incident electron current and smoothed using a 3-point least-squares cubic polynomial algorithm. The symmetry-equivalent beams were then averaged reducing the data set from 23 to 6 inequivalent beams. The total energy range (E_T) defined by the independent experimental beams are 2064 and 1814 eV, respectively, for the 24 ML and 48 ML MnO(100) film thickness.

The LEED analysis was performed using the familiar method of symmetrized automated tensor LEED (Ref. 8) which has been used, for example, to study complex oxide surfaces such as $Fe_3O_4(111)$ (Refs. 9 and 10) and α-$Al_2O_3(0001)$.[11,12] Although MnO is an ionic compound, neutral scattering phase shifts were used. It is well know that the structural fit depends very little on those nonstructural parameters, provided their values are reasonable. Barbieri *et al.*[9] carefully verified this point in a surface structural analysis of $Fe_3O_4(111)$. To take into account the difference in the ionic radii, we assumed that the oxygen muffin-tin radius ($r_{\mathrm{muf}}^{\mathrm{O}}$) was twice the Mn muffin-tin radius ($r_{\mathrm{muf}}^{\mathrm{Mn}}$) in such a way that $r_{\mathrm{muf}}^{\mathrm{O}}+r_{\mathrm{muf}}^{\mathrm{Mn}}=d_{nn}$ where d_{nn} is the nearest-neighbor distance. This was done in order to avoid overlap of the muffin-tin spheres. The muffin-tin potential and the phase shifts were calculated using the Barbieri/Van Hove phase shift package.[13] In particular, a set of 11 relativistic phase shifts ($lmax=10$) was used in all the LEED calculations. In order to quantify the agreement between the experimental and theoretical LEED-IV curves we have used the R factor proposed by Pendry[14] (R_P). All the calculations were performed on the AMD Athlon Oscar/Linux cluster[15] at the surface science laboratory of UFMG.

Since the two MnO films we have quantitatively analyzed in this work were thick enough to totally cover the substrate, we have not considered the Ag(100) in the calculations.

III. RESULTS AND DISCUSSION

The Mn 3*s* doublets of MnO(100) grown films, with thicknesses of 2, 8, and 24 ML, are shown in Fig. 1. The

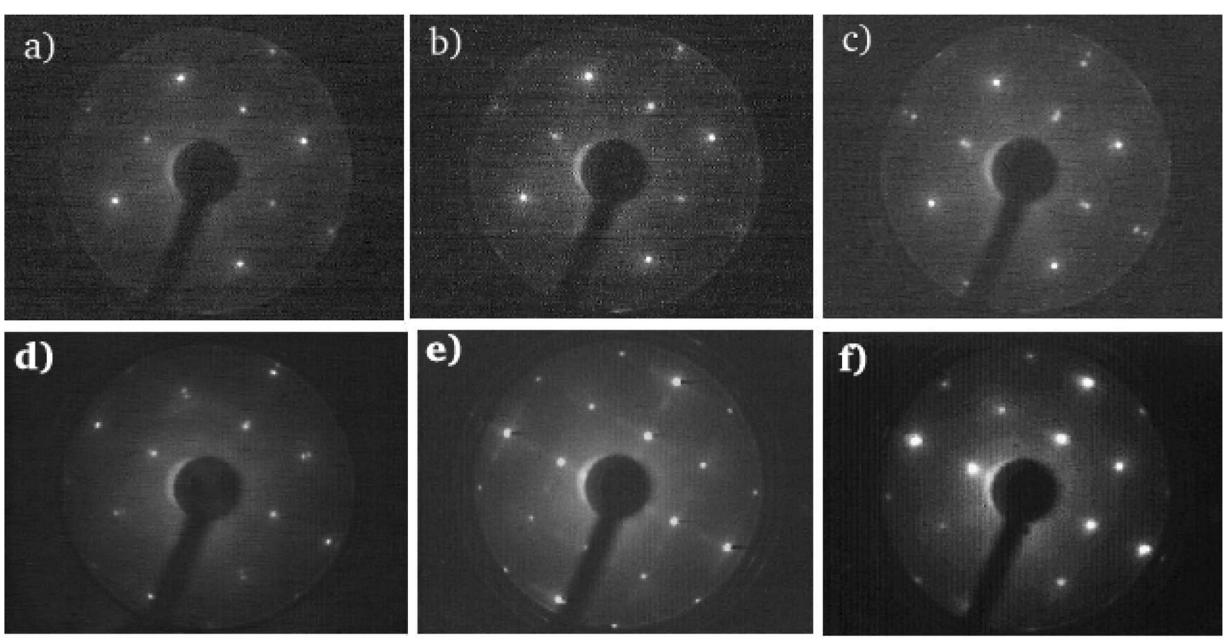

FIG. 2. LEED patterns at 142 eV after annealing the MnO(100) films as a function of the MnO(100) thickness. (a) Clean Ag(100)(1 × 1), (b) 1 ML of MnO(100), (c) 2 ML of MnO(100), (d) 8 ML of MnO(100), (e) 24 ML of MnO(100), and (f) 48 ML of MnO(100).

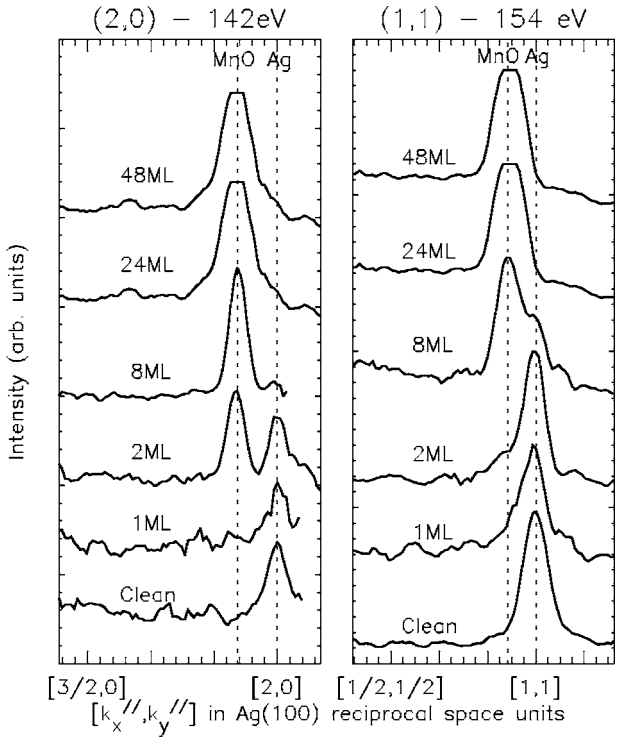

FIG. 3. (2,0) and (1,1) beam profiles along the radial direction at 142 and 154 eV of incidence energy, respectively. $k_x^{//}$ and $k_y^{//}$ are the Ag(100) normalized reciprocal space vectors.

measured energy splitting is the same for all samples (6.10±0.05 eV), exactly the one expected for a pure Mn^{2+} valence state and is in accordance with XPS spectra of MnO grown by other authors.[7,16] We can rule out the formation and coexistence of either Mn_3O_4 or Mn_2O_3 which, having both lower energy splittings, would broaden and turn asymmetric the Mn 3*s* doublet lines of the MnO film. An energy shift towards lower kinetic energy (higher binding energy) is observed for the 24 ML thick sample as compared with the 2 and 8 ML ones, which is obviously due to some surface charging of that sample.

The LEED patterns for the clean Ag(100)(1×1) and for the MnO(100) films after annealing are shown in Fig. 2 as a function of the film thickness at an electron incidence energy of 142 eV. As can be seen from Fig. 2(c), there is a clear splitting of the silver diffracted beams after the growth of 2 ML of MnO(100). A careful analysis of the 2 ML film LEED pattern led us to the conclusion that, in fact, the observed LEED pattern is a superposition of the Ag(100)(1×1) and the MnO(100)(1×1) diffracted patterns with the same orientation. This LEED pattern can be easily explained by assuming that, under our growth conditions, the MnO(100) films grow in islands which are epitaxial to, but incommensurate with, the Ag(100) substrate. The MnO(100) islands cover the substrate only partially, since the diffracted beams from both Ag(100)(1×1) and the MnO(100)(1×1) are visible simultaneously. Estimates of the diffraction angles showed that the pattern related to the MnO(100) film is consistent with a square lattice periodicity around 9% larger than

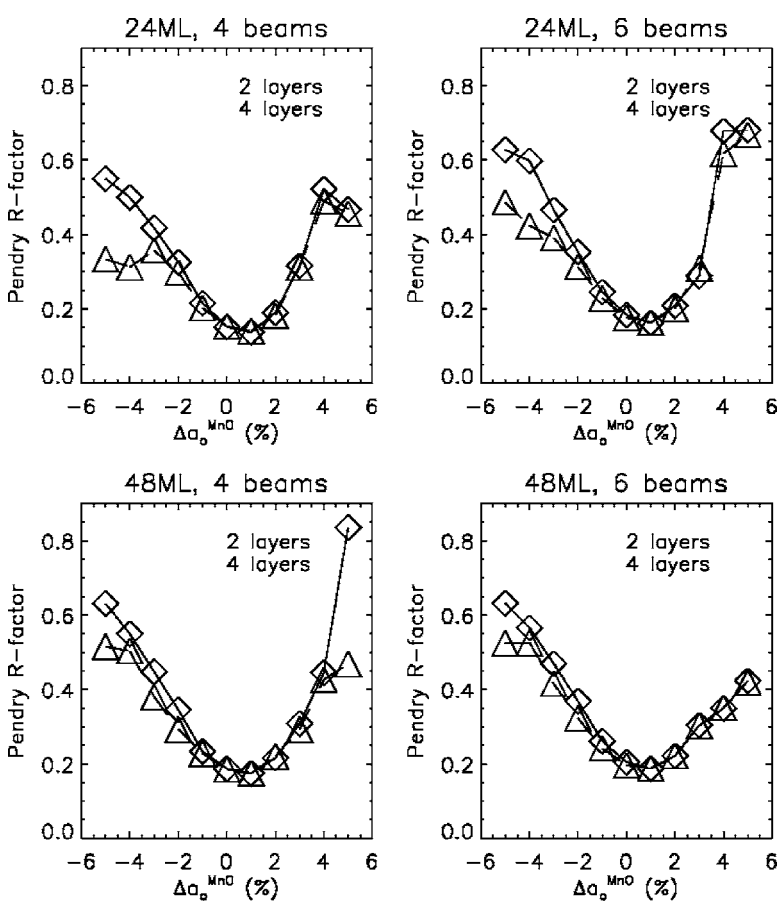

FIG. 4. The behavior of the R_P factor as a function of Δa_0^{MnO} for the 24 ML (top) and 48 ML (bottom) MnO(100) films. Triangles, relaxing two layers. Diamonds, relaxing four layers.

TABLE I. The lowest R_P factor obtained in the lattice constant grid. All of them correspond to a +1% expansion when compared to a single crystal.

Film thickness	24 ML	24 ML	48 ML	48 ML
Expt. beams	4	6	4	6
Four parameters	0.14±0.02	0.16±0.02	0.18±0.03	0.19±0.03
Eight parameters	0.14±0.02	0.16±0.02	0.17±0.03	0.19±0.03

that of Ag(100) which is compatible with the fact that the misfit between Ag and MnO bulk lattice constants is around 8.6%. An equivalent diffraction pattern is also observed for the 8 ML film [Fig. 2(d)]. These observations are in good agreement with the results reported for the growth of 5 ML–7 ML layers of MnO(100) on Ag(100).[7] A similar behavior was observed by Tian *et al.* for the growth of MnO on Cu(100),[17] a system with much larger misfit (23%). It is worth to point out that the same splitting was also visible for the 1 ML thick film but only at incidence energies lower than 100 eV.

After growing 24 ML [Fig. 2(e)] and 48 ML [Fig. 2(f)] of MnO, only the diffracted beams related to the MnO(1×1) were visible indicating that the MnO(100) islands had coalesced totally covering the substrate. This fact can be better seen in Fig. 3 where the spot profiles for the (2,0) and (1,1) beams at incidence energies of 142 eV and 154 eV, respectively, are shown as a function of the film thickness. The spot profiles are measured at a radial direction passing through the diffracted beams using the raw data, i.e., without any smoothing of the curves. It is clear that the intensity of the beams related to the substrate decreases as the film thickness increases. The LEED pattern for the 24 ML film does exhibit some strips between the diffracted spots that may be associated to the existence of mosaics on the surface. It is worth to stress that the six independent experimental LEED-IV curves collected for the 24 ML and 48 ML MnO(100) films are very similar and we should not expect large differences between the structural results obtained from an independent quantitative LEED analysis of the two data sets.

The first issue that we investigated quantitatively was the MnO(100) film in-plane lattice constant (a_0^{MnO}). In order to do that, we have carried out a series of calculations assuming different values for a_0^{MnO} from −5% up to +5% of variation with respect to the MnO(100) single crystal surface lattice constant value of 3.14 Å in steps of 1%. Since we have observed that, under our preparation procedure, the MnO growths nonpseudomorphic even for 1 ML, we have assumed that all layers of the film had the same in-plane lattice constant a_0^{MnO}. For each value of a_0^{MnO}, a full structural optimization was performed starting from the ideal bulk positions. The surface and bulk Debye temperatures were assumed to be identical and equal to 534 K (Ref. 18) in this first step. In order to verify the influence of the number of structural parameters used during the optimization, and the size of the experimental data sets in the final structure, we have carried out the calculations using four and eight fitting parameters (equivalent to relax two and four layers) and four and six experimental beams for the 24 ML and 48 ML films. The R_P factor as a function of the variation of the surface lattice constant ($\Delta a_0^{\mathrm{MnO}}$) with respect to the bulk value is shown in Fig. 4. In all cases, a very well-defined minimum was obtained indicating an expansion of (+1.0±0.6)% of the MnO(100) surface lattice constant. The final structures are also very close to each other suggesting a surface rumple of 0.1 Å with the O^{2-} moving towards the vacuum and the

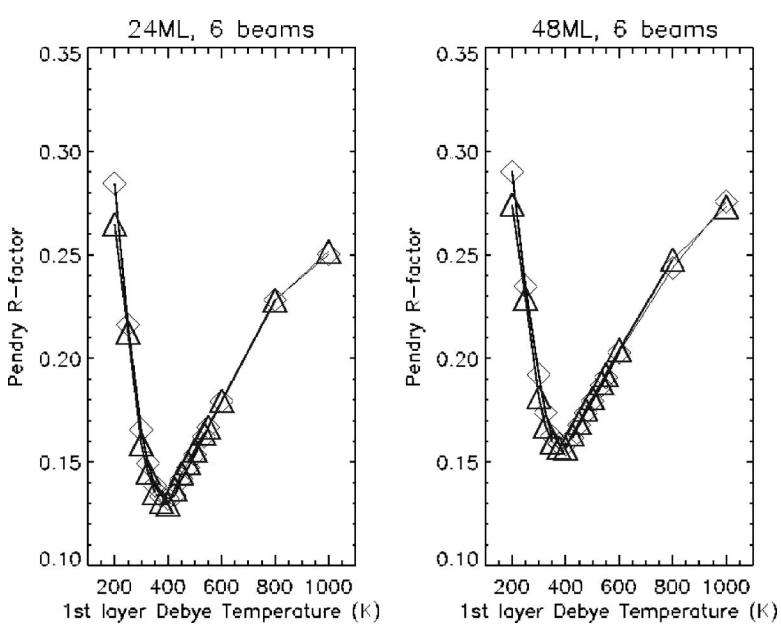

FIG. 5. R_P factor as a function of the surface Debye temperature Θ_1^{MnO} for the 24 ML (left) and 48 ML (right) MnO(100) films. Triangles, relaxing two layers. Diamonds, relaxing four layers.

TABLE II. Final structural parameters after Debye temperature optimization for the 24 ML and 48 ML MnO(100) films. All the calculations were performed using all the six experimental beams and assuming that the Mn^{2+} and O^{2-} have the same Debye temperature in the topmost layer. All the percents are calculated with respect to the optimized film bulk interlayer distance of 2.24 Å, but the Δa_0^{MnO} that is evaluated with respect to the surface lattice constant (3.14 Å) of a MnO single crystal. E_T is the total energy range defined by the independent experimental beams.

MnO(100) thickness	24 ML		48 ML	
Fitting parameters	4	8	4	8
$\Delta a_0^{MnO}(\%)$	1.0±0.6	1.0±0.6	1.0±0.6	1.0±0.6
$\delta_1(\%)$	4.2±1.4	4.1±1.6	5.5±2.5	5.5±2.5
$\Delta_1(\%)$	0.4±1.4	0.3±1.6	1.5±2.5	1.5±2.5
$\delta_2(\%)$	0.2±1.5	0.2±1.7	0.6±2.5	0.5±2.5
$\Delta_2(\%)$	0.3±1.5	0.4±1.7	0.4±2.5	0.4±2.5
$\Delta d_{12}(\%)$	0.1±1.5	−0.1±1.7	1.1±2.5	1.1±2.5
Θ_1^{MnO}(K)	400±80	400±80	400±100	400±100
E_T (eV)	2064	2064	1814	1814
R_P	0.13±0.02	0.13±0.02	0.16±0.02	0.16±0.02

Mn^{2+} moving into the crystal. The rumple in the ith layer is defined as ($\delta_i = \Delta z_i^A - \Delta z_i^C$) where Δz_i^A and Δz_i^C are, respectively, the anion and the cation vertical displacements from the ideal bulk positions. The z-axis points towards the vacuum. The lowest R_P factors obtained are listed in Table I and all of them correspond to an expansion of 1% of the surface lattice constant when compared to the ideal value of a MnO(100) single crystal. It is clear that the expansion in the surface lattice constant and the surface rumple do not depend on the number of fitting parameters or the size of the experimental data set.

Using the optimized geometry found during the lattice constant search as starting point, a grid search over the topmost layer Debye temperature (Θ_1^{MnO}) was conducted over the range 200–1000 K for the 24 ML and 48 ML MnO(100) films. Again, for each value of the Debye temperature, a full optimization of the structural parameters was carried out. The Mn^{2+} and O^{2-} Debye temperatures were assumed to be identical in the topmost layer and all available experimental beams were used in the theory-experiment comparison. The dependence of the R_P factor with Θ_1^{MnO} is shown in Fig. 5. Again, a very well-defined minimum was obtained for each film thickness at Θ_1^{MnO}=400 K (25% lower then the bulk value), independently of the number of fitting parameters and film thickness. In order to try to discriminate the Mn^{2+} and O^{2-} Debye temperatures in the topmost layer a two-dimensional (2D) grid search was also carried out, but the final results for the Debye temperatures were identical to 400 K considering the error bars and no significant improvement in the R_P factor was achieved. The final structural and nonstructural parameters of interest, as well as the corresponding R_P factors are presented in Table II for the two MnO(100) film thicknesses studied here. The relaxation of the ith layer is defined as $\Delta_i = \frac{1}{2}(\Delta z_i^A + \Delta z_i^C)$ and the variation in the interlayer distance between the ith and jth layers can be defined in terms of the layer relaxations as $\Delta d_{ij} = \Delta_i - \Delta_j$. As it can be seen, the final best-fit structures gave very low values for the R_P factors with variances of 0.02. The R_P variance was than used to estimate the error bars of the resulting fitted parameters. The optimized geometries of the MnO(100) films are identical considering the error bars and the most important feature is a surface layer rumple with an average value of δ_1=4.8% (0.11 Å), where the oxygen ions move towards the vacuum and the manganese ions go into the surface. A very small expansion of the first interlayer distance is also observed by LEED, but with large uncertainties. All the other structural parameters can be considered identical to the bulk values. A side view of the MnO(100) film structure is shown in Fig. 6. The comparison between the experimental and theoretical LEED-IV curves for the best models presented in Table II is presented in Fig. 7. It can be seen that there is, indeed, a very good agreement between theory and experiment.

From Table III it can be seen that these results are in agreement with most of the structural studies carried out on the (100) surface of other oxides having the rock-salt struc-

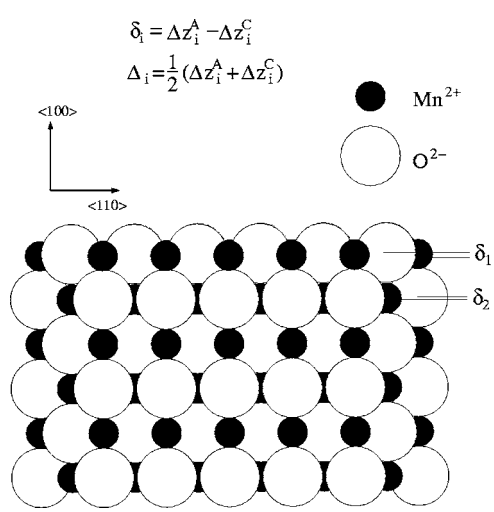

FIG. 6. Side view of the MnO(100) surface structure. The oxygen and manganese ions are represented by the big white and the small black spheres, respectively.

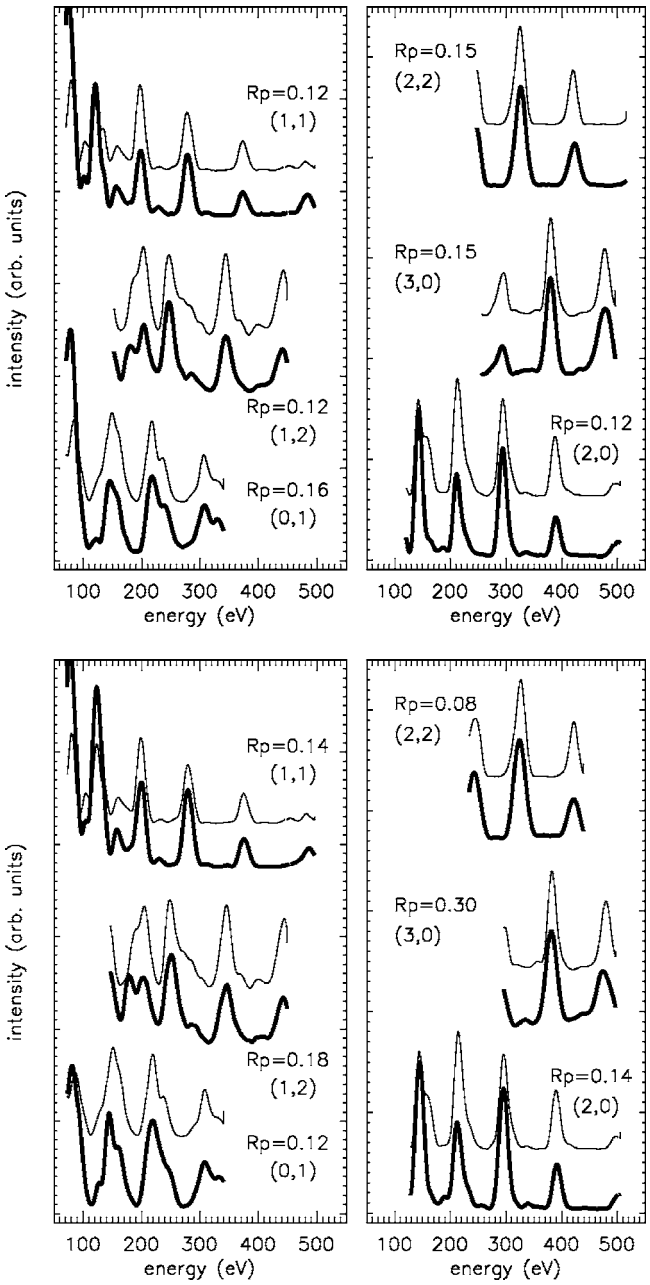

FIG. 7. LEED-IV curves for the 24 ML (top) and 48 ML (bottom) MnO(100) films grown on Ag(100). Thick solid lines, experimental curves. Thin solid lines, theoretical curves for the best model obtained using six beams and relaxing two layers.

ture, but in conflict with the MEIS studies carried out on MnO(100) and NiO(100) single crystals.[4,6] In those studies a rumple of −3.6% and −4.8% were observed for MnO(100) and NiO(100), respectively, but with the O^{2-} ions moving into the bulk. From the MEIS results, it was also possible to derive the individual bulk Debye temperatures (340±30 and 620±50 K for Mn and O, respectively) and the enhancements on the vibration of the topmost layer atoms. In order to explicitly verify if different values for the bulk Debye temperatures would give us different final structures, we have performed all the LEED calculations described above using the values obtained from the MEIS analysis. No significant differences were obtained in this new analysis and final structures are very similar to the one obtained assuming a value of 543 K for the bulk atoms. Indeed, the final R_P factors increased from 0.13 (0.16) to 0.16 (0.21) for the 24 ML (48 ML) MnO(100) film. It is worth to point out that a R_P higher than 0.5 was always obtained when comparing the experimental LEED-IV curves with the theoretical ones calculated from models having the Mn^{2+} ions moving towards the vacuum.

TABLE III. The topmost layer rumple determined for some (100) surfaces of rock-salt oxides obtained by several experimental techniques and theoretical calculations reported in the literature. Experimental results marked with a dagger means that the oxide sample was an ultrathin film grown on a metal substrate and the minus sign represents a displacement of the O^{2-} ions into the crystal (GIXS, represents grazing incidence x-ray scattering).

Oxide	δ_1(Å)	Technique
MnO(100)†	0.10±0.04	LEED (this work)
MnO(100)	−0.08±0.02	MEIS (Ref. 4)
MnO(100)	−0.01	*ab initio* (Ref. 5)
MgO(100)	0.02±0.01	GIXS (Ref. 20)
MgO(100)	0.04±0.04	LEED (Ref. 21)
MgO(100)	0.024	Hartree-Fock (Ref. 22)
NiO(100)†	0.05±0.05	LEED (Ref. 23)
NiO(100)	−0.10±0.01	MEIS (Ref. 6)
NiO(100)	0.014	Hartree-Fock (Ref. 22)
CoO(100)†	0.06±0.04	MEIS (Ref. 24)
CaO(100)	Less then 0.04	LEED (Ref. 25)
Other rock-salt compounds		
NaCl(100)†	0.12±0.03	LEED (Ref. 26)

The rumbles determined by the MEIS studies support recent *ab initio* calculations where the surface properties of MnO(001) and NiO(001) were investigated and contradicts calculations based on semiclassical treatment. It is argued that the disagreement between the semiclassical calculations and the MEIS experiment is due to the fact that pair potentials have an isotropic nature and can only describe almost isotropic electron charge density distributions. This is a good approximation for metallic and ionic compounds and may fail for covalent crystals where there is an accumulation of electrons between the bonding atoms. This type of core-shell approach is basically the one used in LEED to evaluate the phase shifts used to describe the electron scattering inside the crystal. However, it is important to point out that LEED analysis based on the muffin-tin approach for the phase shifts calculations has been used for a long time on the surface structure determination of semiconductors compounds where a reasonable agreement between LEED and *ab initio* calculation were achieved. Very recently, a LEED surface structure determination was performed on the $TiO_2(110)(1\times1)$ where self-consistent phase shifts were used in order to ac-

curately describe the ground state charge density.[19] The use of such type of phase shifts on LEED analysis of MnO(001) films growth on metals may shade some light on the discrepancy between the different experimental results.

IV. CONCLUSIONS

In this work we have successfully applied low energy electron diffraction in order to determine the surface structure of MnO(100) thick films grown on Ag(100). A very good agreement between experiment-theory was obtained as reflected by very low values achieved for the R_P factor. The most important feature observed for the (100) surface of the grown films is a topmost layer rumple of $(4.8\pm2.0)\%$ with the oxygen ions moving towards the vacuum side. These results are in line with other surface structure determinations carried out on the (100) surface of different oxides having rock-salt structure but are in disagreement with MEIS results reported in literature for the MnO(100) using a MnO single crystal and also with the result from recent calculations.

ACKNOWLEDGMENTS

The authors would like to acknowledge the Brazilian research agencies CNPq, FAPEMIG, and the UFMG/PRPq for financial support.

*Electronic address: edmar@fisica.ufmg.br; Present address: CEA - Grenoble, DRFMC, SP2M, 17 rue des Martyrs, 38054. Grenoble Cédex 9, France.

[1] V. E. Henrich and P. A. Cox, *The Surface Science of Metal Oxides* (Cambridge University Press, Cambridge, MA, 1994).
[2] B. Hermsmeier, J. Osterwalder, D. J. Friedman, B. Sinkovic, T. Tran, and C. S. Fadley, Phys. Rev. B **42**, 11895 (1990).
[3] M. A. Langell, C. W. Hutchings, G. A. Carson, and M. H. Nassir, J. Vac. Sci. Technol. A **14**, 1656 (1996).
[4] T. Okazawa and Y. Kido, Surf. Sci. **556**, 101 (2004).
[5] H. Momida and T. Oguchi, J. Phys. Soc. Jpn. **72**, 588 (2003).
[6] T. Okazawa, Y. Yagi, and Y. Kido, Phys. Rev. B **67**, 195406 (2003).
[7] F. Müller, R. Masi, D. Reinicke, P. Steiner, S. Hüfner, and K. Stöwe, Surf. Sci. **520**, 158 (2002).
[8] Barbieri/Van Hove SATLEED package; http://electron.lbl.gov/leedpack/leedpack.html
[9] A. Barbieri, W. Weiss, M. A. Van Hove, and G. Somorjai, Surf. Sci. **302**, 259 (1994).
[10] W. Weiss, A. Barbieri, M. A. Van Hove, and G. A. Somorjai, Phys. Rev. Lett. **71**, 1848 (1993).
[11] C. F. Walters, K. F. McCarty, E. A. Soares, and M. A. Van Hove, Surf. Sci. **464**, L732 (2000).
[12] E. A. Soares, M. A. Van Hove, C. F. Walters, and K. F. McCarty, Phys. Rev. B **65**, 195405 (2002).
[13] Barbieri/Van Hove Phase Shift package; http://electron.lbl.gov/leedpack/leedpack.html
[14] J. B. Pendry, J. Phys. C **13**, 937 (1980).
[15] Open Source Cluster Application Resources (OSCAR); http://oscar.openclustergroup.org/
[16] P. Steiner, R. Zimmermann, F. Reinert, T. Engel, and S. Hiüfner, Z. Phys. B: Condens. Matter **99**, 479 (1996).
[17] D. Tian, H. Li, S. C. Wu, J. Quinn, Y. S. Li, F. Jona, and P. M. Marcus, Phys. Rev. B **46**, 7216 (1992).
[18] O. L. Anderson and D. G. Isaak, *Mineral Physics and Crystallography. A Handbook of Physical Constants* (American Geophysical Union, Washington, DC, 1995).
[19] R. Lindsay, A. Wander, A. Ernst, B. Montanari, G. Thornton, and N. M. Harrison, Phys. Rev. Lett. **94**, 246102 (2005).
[20] O. Robach, G. Renaud, and A. Barbier, Surf. Sci. **401**, 227 (1998).
[21] M. R. Welton-Cook and W. Berndt, J. Phys. C **15**, 5691 (1982).
[22] M. D. Towler, N. M. Harrison, and M. I. McCarthy, Phys. Rev. B **52**, 5375 (1995).
[23] M. Caffio, B. Cortigiani, G. Rovida, A. Atrei, C. Giovanardi, A. di Bona, and S. Valeri, Surf. Sci. **531**, 368 (2003).
[24] J. Wang, K. M. Schindler, W. Widdra, and H. Neddermeyer, ICSOS8 Abstract Book 1, 50 (2005).
[25] M. Prutton, J. A. Ramsey, J. A. Walker, and M. R. Welton-Cook, J. Phys. C **12**, 5271 (1979).
[26] J. G. Roberts, S. Hoffer, M. A. V. Hove, and G. A. Somorjai, Surf. Sci. **437**, 75 (1999).